Adjoint-based formulation for computing derivatives with respect to bed boundary positions in resistivity Geophysics

Théophile Chaumont-Frelet, M Shahrari, D Pardo

ADJOINT-BASED FORMULATION FOR COMPUTING DERIVATIVES WITH RESPECT TO BED BOUNDARY POSITIONS IN RESISTIVITY GEOPHYSICS

T. CHAUMONT-FRELET[1], M. SHAHRARI[1] AND D. PARDO[2,1,3]

Abstract. In inverse geophysical resistivity problems, it is common to optimize for certain resistivity values and bed boundary positions, as needed, for example, in geosteering applications. When using gradient-based inversion methods such as Gauss-Newton, we need to estimate the derivatives of the recorded measurement with respect to the inversion parameters. In this article, we describe an adjoint-based formulation for computing the derivatives of the electric potential and electromagnetic fields with respect to the bed boundary positions. The key idea to obtain this adjoint-based formulation is to separate the tangential and normal components of the field, and treat them differently. We then apply this method to a 1.5D borehole resistivity problem. We illustrate its accuracy and some of its convergence properties via numerical experimentation by comparing those results vs. both the analytical results when available and a finite differences approximation of the derivative.

Keywords. resistivity inversion, adjoint state, potential field inversion, electromagnetic, borehole geophysics

1. Introduction

We consider resistivity measurements to characterize the electrical properties of the subsurface. There exist: (a) *on surface* resistivity measurements acquisition systems such as controlled source electromagnetic (CSEM) [3, 2, 9, 16] and Magnetotellurics (MT) [1, 14], and (b) borehole logging measurements such as those obtained with logging-while-drilling (LWD) devices [21], including the so called deep and extra-deep [17, 8] logging devices used for geosteering purposes [4]. Recently developed LWD resistivity measurements are able to measure all nine components of the magnetic field, namely $\mathcal{H}_{xx}$, $\mathcal{H}_{xy}$, $\mathcal{H}_{xz}$, $\mathcal{H}_{yx}$, $\mathcal{H}_{yy}$, $\mathcal{H}_{yz}$, $\mathcal{H}_{zx}$, $\mathcal{H}_{zy}$, $\mathcal{H}_{zz}$, where the first and second sub-indexes indicate the orientation of the transmitter and the receiver, respectively.

In LWD resistivity measurements, the original Earth's subsurface model is often approximated by a sequence of 1D layer models [7, 15, 13]. Such an approximation often provides reasonable results due to the limited depth of investigation of LWD resistivity measurements compared to the assumed thickness of the geological layers. In presence of a 3D point source, a 1D formation model allows to reduce the dimensionality of the problem from 3D to the so-called 1.5D via a Hankel transform (or two Fourier transforms) [19, 5, 12]. This 1.5D approximation can also be used to obtain an initial subsurface resistivity distribution from marine CSEM measurements [20].

Resistivity measurements are inverted in order to map the Earth's subsurface [15, 9, 7]. Using gradient-based inversion techniques (e.g., Gauss-Newton), we need to estimate the derivatives of the simulated measurements with respect to the inversion variables in order to form the Jacobian matrix. These inversion variables are often the (constant) resistivity values of certain layers and their bed boundary positions. It is well-known how to compute derivatives with respect to the (constant) resistivity values for each layer, both numerically and semi-analytically (see, e.g.,[15, 9, 13, 7, 18]). However, to the best of our knowledge, a fast adjoint-based formulation to compute derivatives with respect to the bed boundary positions in resistivity geophysical problems

[1] Basque Center for Applied Mathematics, (BCAM), Bilbao, Spain
[2] University of the Basque Country (UPV/EHU), Leioa, Spain
[3] Ikerbasque (Basque Foundation for Sciences), Bilbao, Spain .

has not been published before. Such formulation would allow to more rapidly compute accurate approximations of the derivatives than those obtained with a traditional finite differences approach.

The main contribution of this work is to provide an adjoint-state formulation to compute derivatives of resistivity measurements with respect to the bed boundary positions and analyze its performance.. The key idea to obtain such formula is to treat separately the tangential and normal components of the field.

Section 2 introduces notation. In Section 3, we examine the 3D potential equation and derive an adjoint-state formulation to compute the derivative of a measurement with respect to a bed boundary position. The corresponding formulations for 3D Maxwell's equations are provided in Section 4. Section 5 describes the associated 1.5D Maxwell's formulations. We verify and analyze the main advantages and limitations of our adjoint-based method via numerical experimentations in Section 6. Conclusions are in Section 7.

2. Notation

For the sake of simplicity, we focus on the case of a transversally isotropic (TI) media composed of only two layers, separated by a horizontal interface (see Figure 1). Nevertheless, the proposed method easily extends to an arbitrary number of interfaces. In Figure 1, z_i indicates the vertical location of the planar interface that separates the two materials. The conductivity tensor $\boldsymbol{\sigma}_{z_i}$ of the formation is:

$$\boldsymbol{\sigma}_{z_i} = \begin{cases} \boldsymbol{\sigma}^- & z < z_i \\ \boldsymbol{\sigma}^+ & z > z_i \end{cases}, \tag{1}$$

where

$$\boldsymbol{\sigma}^{\pm} = \begin{pmatrix} \sigma_t^{\pm} & 0 & 0 \\ 0 & \sigma_t^{\pm} & 0 \\ 0 & 0 & \sigma_n^{\pm} \end{pmatrix}, \tag{2}$$

and $\sigma_t^{\pm}$ and $\sigma_n^{\pm}$ are positive constants. In (2), subscript t indicates the tangential xy-plane and n the normal component.

We employ a similar notation for vector fields. Thus, if $\boldsymbol{w}$ is a vector, $\boldsymbol{w}_t$ denotes the 2D vector that consists of its two components along the interface plane, and w_n is the normal component.

Figure 1. 1D TI media composed of two different materials.

3. The potential equation

We consider the following 3D potential equation:

$$\begin{aligned} -\nabla \cdot (\boldsymbol{\sigma}_{z_i} \nabla \phi_{z_i}) &= f, \text{ in } \Omega, \\ \phi_{z_i} &= 0, \text{ on } \Gamma = \partial\Omega, \end{aligned} \tag{3}$$

where ϕ_{z_i} is the electric potential, and f is the electric source. Ω is the problem domain and Γ its boundary.

Let v be an arbitrary test function and $\overline{v}$ its complex conjugate. Pre-multiplying (3) by $\overline{v}$ and using integration by parts, we obtain the following variational formulation:

$$b_{z_i}(v, \phi_{z_i}) = \int_\Omega (\nabla \overline{v})^T \boldsymbol{\sigma}_{z_i} \nabla \phi_{z_i} d\boldsymbol{x} = \int_\Omega \overline{v} f d\boldsymbol{x}, \tag{4}$$

where $v, \phi_{z_i} \in H_0^1(\Omega)$, and

$$H_0^1(\Omega) = \{v \in L^2(\Omega) : \nabla v \in \mathbf{L}^2(\Omega), v = 0 \text{ on } \Gamma\}. \tag{5}$$

We assume the measurement of interest $m = m(z_i)$ depends linearly on ϕ_{z_i}. Hence, we have:

$$m(z_i) := \int_\Omega \overline{g}\phi_{z_i} d\boldsymbol{x}, \tag{6}$$

for some g, where the dependence upon z_i is explicit in the notation.

In order to obtain the adjoint-based formula that expresses the derivative of the measurements, it is convenient to introduce the adjoint solution $\phi^*_{z_i}$, which satisfies:

$$b_{z_i}(\phi^*_{z_i}, v) = \int_\Omega \overline{g} v d\boldsymbol{x}, \ \forall v \in H^1_0(\Omega). \tag{7}$$

An important property of the adjoint solution is that we have:

$$b_{z_i}(\phi^*_{z_i}, \phi_{z_i}) = m(z_i). \tag{8}$$

We emphasize that (7) and (8) are valid for any interface position z_i.

In the following, we obtain an expression for the derivative of m with respect to z_i using the adjoint state method. To this end, we introduce a small perturbation ϵ for a given position z_i. Since the right-hand-side of (7) is independent of the trial function, for the test function $v = \phi_{z_i+\epsilon}$, we obtain:

$$b_{z_i+\epsilon}(\phi^*_{z_i+\epsilon}, \phi_{z_i+\epsilon}) = b_{z_i}(\phi^*_{z_i}, \phi_{z_i+\epsilon}). \tag{9}$$

Similarly, by using (4), we have:

$$b_{z_i}(\phi^*_{z_i}, \phi_{z_i}) = b_{z_i+\epsilon}(\phi^*_{z_i}, \phi_{z_i+\epsilon}). \tag{10}$$

Hence, we have the following:

(11)

$$\begin{aligned} m(z_i+\epsilon) - m(z_i) = b_{z_i}(\phi^*_{z_i}, \phi_{z_i+\epsilon}) - b_{z_i+\epsilon}(\phi^*_{z_i}, \phi_{z_i+\epsilon}) &= \int_\Omega \left(\nabla\overline{\phi^*_{z_i}}\right)^T (\boldsymbol{\sigma}_{z_i} - \boldsymbol{\sigma}_{z_i+\epsilon}) \nabla\phi_{z_i} d\Omega \\ &= \int_{\boldsymbol{x}_t} \int_{z_i}^{z_i+\epsilon} \left(\nabla\overline{\phi^*_{z_i}}\right)^T (\boldsymbol{\sigma}^- - \boldsymbol{\sigma}^+) \nabla\phi_{z_i} dx_n d\boldsymbol{x}_t. \end{aligned}$$

At this point, the normal and tangential components of the gradients have to be treated separately since they satisfy different compatibility conditions across the interface, namely:

$$[(\nabla\phi_{z_i+\epsilon})_t]_{z_i+\epsilon} = \boldsymbol{0}, \quad [\sigma_{n,z_i+\epsilon}(\nabla\phi_{z_i+\epsilon})_n]_{z_i+\epsilon} = 0, \tag{12}$$

where, for ψ and $\tilde{z}$,

$$[\psi(\boldsymbol{x})]_{\tilde{z}} = \lim_{x_n \to \tilde{z}^+} \psi(\boldsymbol{x}_t, x_n) - \lim_{x_n \to \tilde{z}^-} \psi(\boldsymbol{x}_t, x_n) \tag{13}$$

denotes the jump of ψ across the interface located at $\tilde{z}$. Then, we rewrite (11) as

$$\begin{aligned} m(z_i+\epsilon) - m(z_i) &= \int_{\boldsymbol{x}_t} \int_{z_i}^{z_i+\epsilon} (\nabla\overline{\phi^*_{z_i}})^T_t (\sigma_{t,z_i} - \sigma_{t,z_i+\epsilon})(\nabla\phi_{z_i+\epsilon})_t dx_n d\boldsymbol{x}_t \\ &\quad + \int_{\boldsymbol{x}_t} \int_{z_i}^{z_i+\epsilon} (\nabla\overline{\phi^*_{z_i}})^T_n (\sigma_{n,z_i} - \sigma_{n,z_i+\epsilon})(\nabla\phi_{z_i+\epsilon})_n dx_n d\boldsymbol{x}_t \\ &= \int_{\boldsymbol{x}_t} \int_{z_i}^{z_i+\epsilon} (\nabla\overline{\phi^*_{z_i}})^T_t (\sigma_{t,z_i} - \sigma_{t,z_i+\epsilon})(\nabla\phi_{z_i+\epsilon})_t dx_n d\boldsymbol{x}_t \\ &\quad - \int_{\boldsymbol{x}_t} \int_{z_i}^{z_i+\epsilon} (\rho_{n,z_i} - \rho_{n,z_i+\epsilon}) \left(\sigma_{n,z_i} \nabla\overline{\phi^*_{z_i}}\right)^T_n (\sigma_{n,z_i+\epsilon} \nabla\phi_{z_i+\epsilon})_n \, dx_n d\boldsymbol{x}_t, \end{aligned} \tag{14}$$

where $\rho_{n,z_i} = (\sigma_{n,z_i})^{-1}$.

Recalling (12), we have:

$$\left(\nabla\boldsymbol{\phi}_{z_i+\epsilon}\right)_t = (\nabla\boldsymbol{\phi}_{z_i})_t + o(\epsilon), \quad \left(\sigma_{n,z_i+\epsilon}\nabla\boldsymbol{\phi}_{z_i+\epsilon}\right)_n = \left(\sigma_{n,z_i}\nabla\boldsymbol{\phi}_{z_i}\right)_n + o(\epsilon). \tag{15}$$

Then, using Taylor's series expansion, we show that for any smooth function ψ, we have:

(16)
$$\begin{aligned}\int_\Omega (\sigma_{t,z_i} - \sigma_{t,z_i+\epsilon})\psi(\boldsymbol{x}_t, z)d\boldsymbol{x} &= \int_{\boldsymbol{x}_t}\int_{z_i}^{z_i+\epsilon} (\sigma_{t,z_i} - \sigma_{t,z_i+\epsilon})\psi(\boldsymbol{x}_t, z)dx_n d\boldsymbol{x}_t = \int_{\boldsymbol{x}_t}\int_{z_i}^{z_i+\epsilon} [\sigma_t]\left(\psi(\boldsymbol{x}_t, z_i) + o(\epsilon)\right)dx_n d\boldsymbol{x}_t \\ &= \int_{\boldsymbol{x}_t} \epsilon[\sigma_t]\left(\psi(\boldsymbol{x}_t, z_i) + o(\epsilon)\right)d\boldsymbol{x}_t = \epsilon[\sigma_t]\int_{\Gamma_i}\psi(\boldsymbol{x}_t, z_i)d\Gamma_i + o(\epsilon^2),\end{aligned}$$

where $\Gamma_i = \{\boldsymbol{x} \in \Omega :\ x_n = z_i\}$ is the interface between the two materials. Following an analogous argument for the normal component, we obtain:

(17)
$$\frac{m(z_i+\epsilon) - m(z_i)}{\epsilon} = [\sigma_t]\int_{\Gamma_i}\left(\nabla\overline{\phi^*_{z_i}}\right)_t^T(\nabla\phi_{z_i})_t\, d\Gamma_i - [\rho_n]\int_{\Gamma_i}\left(\sigma_{n,z_i}\nabla\overline{\phi^*_{z_i}}\right)_n^T(\sigma_{n,z_i}\nabla\phi_{z_i})_n\, d\Gamma_i + o(\epsilon),$$

where

$$[\sigma_t] = \sigma_t^+ - \sigma_t^-, \quad [\rho_n] = (\sigma_n^+)^{-1} - (\sigma_n^-)^{-1}. \tag{18}$$

Hence, letting $\epsilon \to 0$, we have:

$$\frac{dm}{dz_i}(z_i) := [\sigma_t]\int_{\Gamma_i}\left(\nabla\overline{\phi^*_{z_i}}\right)_t^T(\nabla\phi_{z_i})_t\, d\Gamma_i - [\rho_n]\int_{\Gamma_i}\left(\sigma_{n,z_i}\nabla\overline{\phi^*_{z_i}}\right)_n^T(\sigma_{n,z_i}\nabla\phi_{z_i})_n\, d\Gamma_i. \tag{19}$$

4. Maxwell's equations

In this section, we consider 3D Maxwell's equations to model the EM fields [11, 6]. Then, for a given interface position z_i, we have:

$$\nabla \times \boldsymbol{\mathcal{H}}_{z_i} = \tilde{\boldsymbol{\sigma}}_{z_i}\boldsymbol{\mathcal{E}}_{z_i}, \tag{20}$$

$$\nabla \times \boldsymbol{\mathcal{E}}_{z_i} = i\omega\boldsymbol{\mu}\boldsymbol{\mathcal{H}}_{z_i} + i\omega\boldsymbol{\mu}\mathbf{M}, \tag{21}$$

where $\boldsymbol{\mathcal{E}}_{z_i}$ is the complex-valued electric field, $\boldsymbol{\mathcal{H}}_{z_i}$ is the magnetic field, $\omega = 2\pi f$ is the angular frequency, where $f > 0$ is the frequency of the transmitter, and $\tilde{\boldsymbol{\sigma}}_{z_i} = \boldsymbol{\sigma}_{z_i} - i\omega\boldsymbol{\varepsilon}$, where $\boldsymbol{\varepsilon}$ is the permittivity tensor of the medium and i is the imaginary unit, and $\boldsymbol{\mu}$ is the magnetic permeability tensor of the media. For the sake of simplicity, we consider the case where $\boldsymbol{\varepsilon} = \varepsilon_0\mathbf{I}_3$ and $\boldsymbol{\mu} = \mu_0\mathbf{I}_3$ with $\mathbf{I}_3$ being the 3D identity matrix, and ε_0 and μ_0 are the vacuum permittivity and permeability, respectively. To simplify derivations, we consider the whole 3D space as our domain, so that the problem is set on $\Omega = \mathbb{R}^3$.

Though it is possible to solve problem (20)-(21) directly, it is generally recast as a second order system. For instance, by applying the curl operator to (20) and substituting (21) into the result, we arrive at the magnetic field formulation:

$$\nabla \times \left(\tilde{\boldsymbol{\sigma}}_{z_i}^{-1}\nabla \times \boldsymbol{\mathcal{H}}_{z_i}\right) - i\omega\boldsymbol{\mu}\boldsymbol{\mathcal{H}}_{z_i} = i\omega\boldsymbol{\mu}\mathbf{M}. \tag{22}$$

The above equation is complemented with the condition that the electromagnetic fields are expected to decrease sufficiently fast when increasing the distance to the transmitter.

4.1. Weak formulation.

Let $\boldsymbol{\mathcal{F}}$ be an arbitrary test function and $\overline{\boldsymbol{\mathcal{F}}}^T$ its conjugate transpose. Pre-multiplying Equation (22) by $\overline{\boldsymbol{\mathcal{F}}}^T$ and integrating over domain Ω, we obtain:

$$\int_\Omega \overline{\boldsymbol{\mathcal{F}}}^T(\nabla \times \tilde{\boldsymbol{\sigma}}_{z_i}^{-1}\nabla \times \boldsymbol{\mathcal{H}}_{z_i})d\Omega - i\omega\mu_0\int_\Omega \overline{\boldsymbol{\mathcal{F}}}^T\boldsymbol{\mathcal{H}}_{z_i}d\Omega = i\omega\mu_0\int_\Omega \overline{\boldsymbol{\mathcal{F}}}^T\mathbf{M}d\Omega. \tag{23}$$

We select $\boldsymbol{\mathcal{F}} \in H(\mathbf{curl}; \Omega)$, where:

$$H(\mathbf{curl}; \Omega) = \{\boldsymbol{\mathcal{F}} \in \mathbf{L}^2(\Omega) : \nabla \times \boldsymbol{\mathcal{F}} \in \mathbf{L}^2(\Omega)\}.$$

Using integration by parts:

$$b_{z_i}(\boldsymbol{\mathcal{F}}, \boldsymbol{\mathcal{H}}_{z_i}) = i\omega\mu_0\int_\Omega \overline{\boldsymbol{\mathcal{F}}}^T\mathbf{M}d\Omega, \tag{24}$$

where

$$b_{z_i}(\boldsymbol{\mathcal{F}}, \boldsymbol{\mathcal{H}}_{z_i}) = \int_\Omega (\nabla \times \overline{\boldsymbol{\mathcal{F}}})^T (\tilde{\boldsymbol{\sigma}}_{z_i}^{-1} \nabla \times \boldsymbol{\mathcal{H}}_{z_i}) d\Omega - i\omega\mu_0 \int_\Omega \overline{\boldsymbol{\mathcal{F}}}^T \boldsymbol{\mathcal{H}}_{z_i} d\Omega, \tag{25}$$

and $\boldsymbol{\mathcal{H}}_{z_i} \in H(\mathbf{curl}; \Omega)$. We assume that the measurements are given by:

$$m(z_i) = \int_\Omega \overline{\mathbf{K}}^T \boldsymbol{\mathcal{H}}_{z_i}, \tag{26}$$

for some $\mathbf{K}$. Continuity of the electric displacement implies the following compatibility conditions:

$$\begin{aligned} &[(\boldsymbol{\mathcal{E}}_{z_i+\epsilon})_t]_{z_i+\epsilon} = \mathbf{0}, \\ &[\tilde{\sigma}_{n,z_i+\epsilon} (\boldsymbol{\mathcal{E}}_{z_i+\epsilon})_n]_{z_i+\epsilon} = 0, \end{aligned} \tag{27}$$

where $\tilde{\sigma}_{n,z_i} = \sigma_{n,z_i} - i\omega\varepsilon_0$. By using (20), we obtain the following compatibility conditions for the magnetic field:

$$\begin{aligned} &[\tilde{\rho}_{t,z_i+\epsilon} (\nabla \times \boldsymbol{\mathcal{H}}_{z_i+\epsilon})_t]_{z_i+\epsilon} = \mathbf{0}, \\ &[(\nabla \times \boldsymbol{\mathcal{H}}_{z_i+\epsilon})_n]_{z_i+\epsilon} = 0, \end{aligned} \tag{28}$$

where $\tilde{\rho}_{t,z_i} = (\tilde{\sigma}_{t,z_i})^{-1}$ and $\tilde{\sigma}_{t,z_i} = \sigma_{t,z_i} - i\omega\varepsilon_0$. The adjoint solution $\boldsymbol{\mathcal{H}}^*_{z_i}$ is the solution to:

$$b_{z_i}(\boldsymbol{\mathcal{H}}^*_{z_i}, \boldsymbol{\mathcal{F}}) = \int_\Omega \overline{\mathbf{K}}^T \boldsymbol{\mathcal{F}}, \ \forall \boldsymbol{\mathcal{F}} \in H(\mathbf{curl}; \Omega). \tag{29}$$

Similarly to the potential equation, our adjoint solution satisfies the following variational formulation:

$$b_{z_i}(\boldsymbol{\mathcal{H}}^*_{z_i}, \boldsymbol{\mathcal{H}}_{z_i}) = m(z_i) \tag{30}$$

Following an analogous derivation as for the potential equation, we obtain:

(31)

$$\frac{dm}{dz_i}(z_i) = [\tilde{\sigma}_t] \int_{\Gamma_{z_i}} \left(\tilde{\rho}_{t,z_i} \left(\nabla \times \overline{\boldsymbol{\mathcal{H}}^*_{z_i}} \right)_t \right)^T (\tilde{\rho}_{t,z_i} (\nabla \times \boldsymbol{\mathcal{H}}_{z_i})_t) \, d\Gamma_{z_i} - [\tilde{\rho}_n] \int_{\Gamma_{z_i}} (\nabla \times \overline{\boldsymbol{\mathcal{H}}^*_{z_i}})^T_n (\nabla \times \boldsymbol{\mathcal{H}}_{z_i})_n d\Gamma_{z_i},$$

where

$$[\tilde{\sigma}_t] = \sigma_t^+ - \sigma_t^-, \quad [\tilde{\rho}_n] = (\sigma_n^+ - i\omega\varepsilon_0)^{-1} - (\sigma_n^- - i\omega\varepsilon_0)^{-1}. \tag{32}$$

5. 1.5D formulation

We consider the magnetic field in the Cartesian system of coordinates as $\boldsymbol{\mathcal{H}}_{z_i} = (\mathcal{H}_{x,z_i}, \mathcal{H}_{y,z_i}, \mathcal{H}_{z,z_i})$. For problems where material properties vary only in the z-direction, it is convenient to use a 2D Fourier transform along the xy-plane. We consider $\widehat{\boldsymbol{H}}_{z_i}$ to be the 2D Fourier transform of $\boldsymbol{\mathcal{H}}_{z_i}$ along x and y directions. We have:

$$\boldsymbol{\mathcal{H}}_{z_i}(\boldsymbol{x}_t, x_n) := \frac{1}{4\pi^2} \int_{-\infty}^{+\infty} \int_{-\infty}^{+\infty} \widehat{\boldsymbol{H}}_{z_i}(\boldsymbol{k}, x_n) e^{i\boldsymbol{k}\cdot\boldsymbol{x}_t} d\boldsymbol{k}, \tag{33}$$

where $\boldsymbol{k} = (k_x, k_y)$. We change the system of coordinates from the Cartesian to a cylindrical one according to the following transformations:

$$\begin{aligned} &x = \rho \cdot \cos\phi, \ y = \rho \cdot \sin\phi, \\ &k_x = \xi \cdot \cos\theta, \ k_y = \xi \cdot \sin\theta. \end{aligned} \tag{34}$$

Substituting (34) into (33), we obtain:

$$\boldsymbol{\mathcal{H}}_{z_i}(\boldsymbol{\rho}) = \frac{1}{4\pi^2} \int_0^{+\infty} \int_0^{2\pi} \widehat{\boldsymbol{H}}_{z_i}(\xi, \theta, x_n) e^{i\xi\rho(\cos\theta\cos\phi + \sin\theta\sin\phi)} d\theta\xi d\xi, \tag{35}$$

where $\boldsymbol{\rho} = (\rho, \phi, x_n)$. Using the identity $\cos(\phi - \theta) = \cos\theta\cos\phi + \sin\theta\sin\phi$, we arrive at:

$$\boldsymbol{\mathcal{H}}_{z_i}(\boldsymbol{\rho}) = \frac{1}{4\pi^2} \int_0^{+\infty} \int_0^{2\pi} \widehat{\boldsymbol{H}}_{z_i}(\xi, \theta, x_n) e^{i\xi\rho\cos(\phi-\theta)} d\theta\xi d\xi. \tag{36}$$

We have the following relation between exponentials and Bessel functions:

$$e^{i\xi\rho\cos(\phi-\theta)} = \sum_{r=-\infty}^{\infty} i^r J_r(\xi\rho)e^{-ir(\phi-\theta)}. \tag{37}$$

Substituting (37) into (36), we obtain:

$$\boldsymbol{\mathcal{H}}_{z_i}(\boldsymbol{\rho}) = \frac{1}{2\pi}\sum_{r=-\infty}^{\infty}\int_0^{+\infty} \boldsymbol{H}^r_{z_i}(\xi, x_n)J_r(\xi\rho)e^{-ir\phi}\xi d\xi, \tag{38}$$

where

$$\boldsymbol{H}^r_{z_i}(\xi, x_n) = \frac{1}{2\pi}\int_0^{2\pi} \widehat{\boldsymbol{H}}_{z_i}(\xi, \theta, x_n)i^r e^{ir\theta}d\theta. \tag{39}$$

Analogously, we consider the adjoint solution as follows:

$$\boldsymbol{\mathcal{H}}^*_{z_i}(\boldsymbol{\rho}) = \frac{1}{2\pi}\sum_{r=-\infty}^{\infty}\int_0^{+\infty} \boldsymbol{H}^{*,r}_{z_i}(\xi, x_n)J_r(\xi\rho)e^{-ir\phi}\xi d\xi, \tag{40}$$

For an arbitrary function $\mathbf{g}(\xi, z) = (g_x(\xi, x_n), g_y(\xi, x_n), g_z(\xi, x_n))$ in the spectral domain, we define:

$$\begin{aligned} g_+(\xi, x_n) &= \frac{g_x(\xi, x_n) - ig_y(\xi, x_n)}{2}, \\ g_-(\xi, x_n) &= \frac{g_x(\xi, x_n) + ig_y(\xi, x_n)}{2}, \end{aligned} \tag{41}$$

and

$$\begin{aligned} \Pi^{\xi}_{+}\left(\mathbf{g}(\xi, x_n)\right) &:= \frac{\partial g_+(\xi, x_n)}{\partial z} + \frac{\xi}{2}g_z(\xi, x_n), \\ \Pi^{\xi}_{-}\left(\mathbf{g}(\xi, x_n)\right) &:= \frac{\partial g_-(\xi, x_n)}{\partial z} - \frac{\xi}{2}g_z(\xi, x_n), \\ \Pi^{\xi}_{z}\left(\mathbf{g}(\xi, x_n)\right) &= \xi\left(g_-(\xi, x_n) + g_+(\xi, x_n)\right). \end{aligned} \tag{42}$$

Using the Hankel representation given by Equation (40), and proper orthogonality properties of Bessel functions, Equation (25) reduces to:

$$b(\boldsymbol{\mathcal{F}}^{q,m}, \boldsymbol{\mathcal{H}}) = b(\mathbf{F}^m, \mathbf{H}^m) = b_1(\mathbf{F}^m, \mathbf{H}^m) - b_2(\mathbf{F}^m, \mathbf{H}^m), \tag{43}$$

where

(44)

$$\begin{aligned} b_1(\mathbf{F}^m, \mathbf{H}^m) =& 2\langle \Pi^{\xi_q}_{-}\left(\mathbf{F}^m\right), \tilde{\sigma}^{-1}_{z_i}\Pi^{\xi_q}_{-}\left(\mathbf{H}^m\right)\rangle_{L^2} + 2\langle \Pi^{\xi_q}_{+}\left(\mathbf{F}^m\right), \tilde{\sigma}^{-1}_{h}\Pi^{\xi_q}_{+}\left(\mathbf{H}^m\right)\rangle_{L^2} + \langle \Pi^{\xi_q}_{z}\left(\mathbf{F}^m\right), \tilde{\sigma}^{-1}_{v}\Pi^{\xi_q}_{z}\left(\mathbf{H}^m\right)\rangle_{L^2}, \\ b_2(\mathbf{F}^m, \mathbf{H}^m) =& i\omega\mu_0\left(2\langle F^m_-, H^m_-\rangle_{L^2} + 2\langle F^m_+, H^m_+\rangle_{L^2} + \langle F^m_z, H^m_z\rangle_{L^2}\right). \end{aligned}$$

and $\langle f, g\rangle_{L^2} = \int_z \bar{f}g dz$. For the above formulation to be integrable, we need $\mathbf{H}^m, \mathbf{F}^m \in V(\mathbb{R})$, where $V(\mathbb{R}) = H^1(\mathbb{R}) \times H^1(\mathbb{R}) \times L^2(\mathbb{R})$, and

$$H^1(\mathbb{R}) = \{v \in L^2(\mathbb{R}) : \frac{\partial v}{\partial z} \in L^2(\mathbb{R})\}. \tag{45}$$

For a detailed derivation of the 1.5D variational formulation, see [19]. Using (44), the derivative of the magnetic field with respect to boundary position becomes:

$$\begin{aligned} \frac{dm}{dz_i}(z_i) =& 2[\tilde{\sigma}_{t,z_i}]_{z_i}\left(\tilde{\rho}_{t,z_i}\overline{\Pi^{\xi_q}_{-}(\boldsymbol{H}^{*,m}_{z_i})}\tilde{\rho}_{t,z_i}\Pi^{\xi_q}_{-}(\boldsymbol{H}^m_{z_i}) + \tilde{\rho}_{t,z_i}\overline{\Pi^{\xi_q}_{+}(\boldsymbol{H}^{*,m}_{z_i})}\tilde{\rho}_{t,z_i}\Pi^{\xi_q}_{+}(\boldsymbol{H}^m_{z_i})\right)(z_i) \\ &- [\tilde{\rho}_{n,z_i}]_{z_i}\left(\overline{\Pi^{\xi_q}_{z}\left(\boldsymbol{H}^{*,m}_{z_i}\right)}\Pi^{\xi_q}_{z}\left(\boldsymbol{H}^m_{z_i}\right)\right)(z_i). \end{aligned} \tag{46}$$

6. Numerical experiments

6.1. **Model problem A: 2D potential equation.** We consider a 2D potential equation set in the unit square $\Omega = (0,1)^2$:

$$-\nabla \cdot (\boldsymbol{\sigma}_{z_i} \nabla \phi_{z_i}) = f, \tag{47}$$

where f is a given right-hand-side and $\boldsymbol{\sigma}_{z_i} = \sigma_{z_i} \mathbf{I}_2$, where

$$\sigma_{z_i}(\boldsymbol{x}) = \begin{cases} \sigma_- & \text{if } z < z_i \\ \sigma_+ & \text{if } z > z_i \end{cases} \tag{48}$$

is the conductivity of a 1D layered media that consist of two different layers, and $\sigma_\pm$ are two positive values. In this example, we consider $\sigma_- = 1 Sm^{-1}$ and $\sigma_+ = 10 Sm^{-1}$, and $f = -2$. The boundary conditions are:

$$\phi_{z_i}(x,0) = \frac{\partial \phi_{z_i}}{\partial z}(x,1) = 0, \quad \frac{\partial \phi_{z_i}}{\partial x}(0,z) = \frac{\partial \phi_{z_i}}{\partial x}(1,z) = 0. \tag{49}$$

The analytical solution for this problem is:

$$\phi_{z_i}(\boldsymbol{x}) = \begin{cases} \rho_- z(z-2) & \text{if } z < z_i \\ \rho_+ z(z-2) - [\rho] z_i (z_i - 2) & \text{if } z > z_i. \end{cases} \tag{50}$$

In addition, we fix $g = -2$. Therefore, the direct and adjoint solutions are the same, and we have:

$$m(z_i) = -2 \int_\Omega \phi_{z_i}(x,z) d\Omega = -2[\rho] \left(\frac{2}{3} z_i^3 - 2 z_i^2 + 2 z_i \right) + \frac{4}{3} \rho_+, \tag{51}$$

as well as

$$\frac{dm}{dz_i}(z_i) = -4[\rho] \left(z_i - 1 \right)^2. \tag{52}$$

Figure 2 compares the derivative of m computed using adjoint state expression (19) vs the analytical expression (52). As shown there, the numerical result is highly accurate. Figure 3 analyses the convergence of the adjoint-based gradient with respect to the finite element mesh size for the case $z_i = 0.5$, and we observe a linear convergence rate.

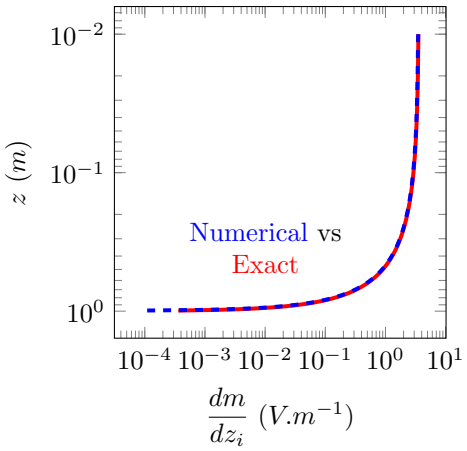

Figure 2. Model problem A. Analytical and numerical gradient.

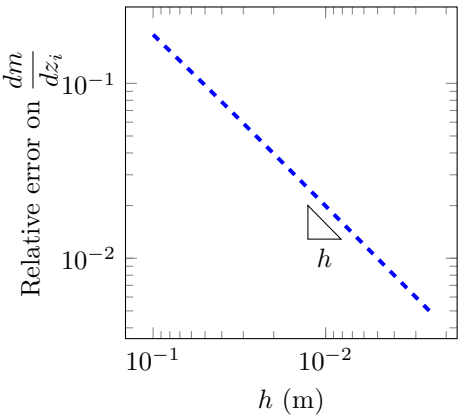

FIGURE 3. Model problem A. Convergence of the numerical gradient at point $z_i = 0.5$.

6.2. **1.5D borehole application.** For Maxwell's equation, we consider $\mathbf{K}$ and $\mathbf{M}$ to be vectorial delta distributions corresponding to point sources. We use the multi-scale Hankel finite element method implemented in FORTRAN 90 and described in [19] to compute the derivatives given by Equation (46). We use a fast inverse Hankel transform based on digital filters to transfer our solution to the space domain (see [10] for details). Moreover, to have a tractable computational domain, we truncate it along z direction with $\Omega_z = (z_0, z_1)$. Since the magnetic field decays exponentially fast as we move away from the transmitter, we impose a zero Drichlet boundary condition at $z = z_0$ and at $z = z_1$.

In addition, for the sake of simplicity, we consider coaxial tools in a vertical well. As a result, the transmitter and receiver are oriented along the z axis, and we have $\mathbf{K} = (0, 0, \delta_{Rx})$, $\mathbf{M} = (0, 0, \delta_{Tx})$, where Rx and Tx respectively denote the position of the receiver and transmitter.

We only make these assumptions to simplify the presentation. It is possible to consider triaxial tools with general trajectories.

6.2.1. *Model problem B: two-layer media.* Figure 4 describes the logging instrument used in this model problem. The conductivity of the two-layer media is given by $\boldsymbol{\sigma}_{z_i} = \sigma_{z_i}\mathbf{I}_3$, where:

$$\sigma_{z_i}(\boldsymbol{x}) = \begin{cases} 1 & Sm^{-1} \quad \text{if } 0 < z < z_i \\ 10^{-2} & Sm^{-1} \quad \text{if } z_i \leq z < 6, \end{cases} \tag{53}$$

and $z_i = 3.15\ m$.

In this example, the measurement is the value of the z component of the magnetic field at the receiver. To simplify notation, we denote $\mathcal{H} = \mathcal{H}_{z_i,z}(Rx)$ to the recorded value, and we have $m(z_i) = \mathcal{H}$.

Figure 5 shows the real and imaginary parts, and the absolute value of $\mathcal{H}$ for different tool positions. Figure 6 compares the derivative with respect to the bed boundary position using the 1.5D adjoint formulation (46) vs that obtained with a finite differences approximation. The finite differences approximation experiences some oscillations due to numerical errors. The solution using the adjoint state method shows superior accuracy and avoids any spurious oscillation.

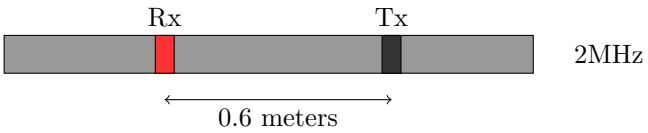

FIGURE 4. Model problem B. Logging instrument. Tx and Rx denote the transmitter and the receiver, respectively.

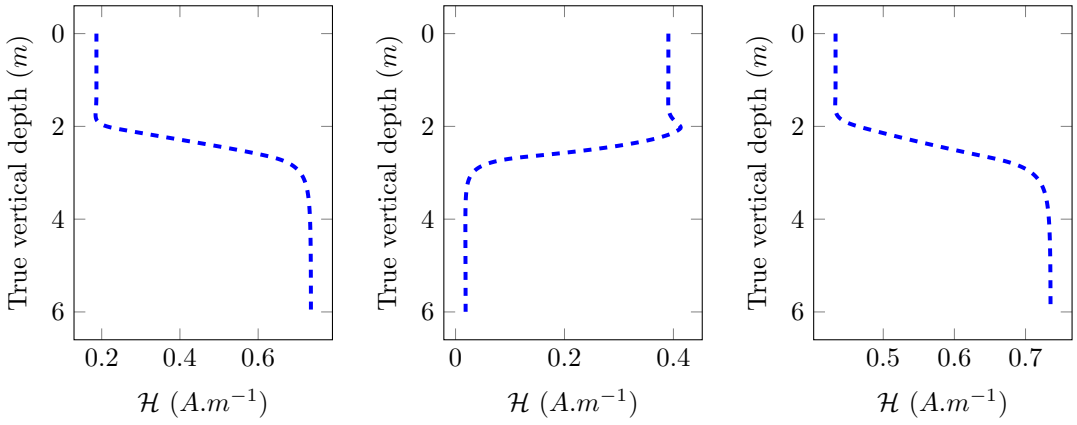

(A) Real part (B) Imaginary part (C) Absolute value

FIGURE 5. Model problem B. zz-component of the magnetic field for a vertical well.

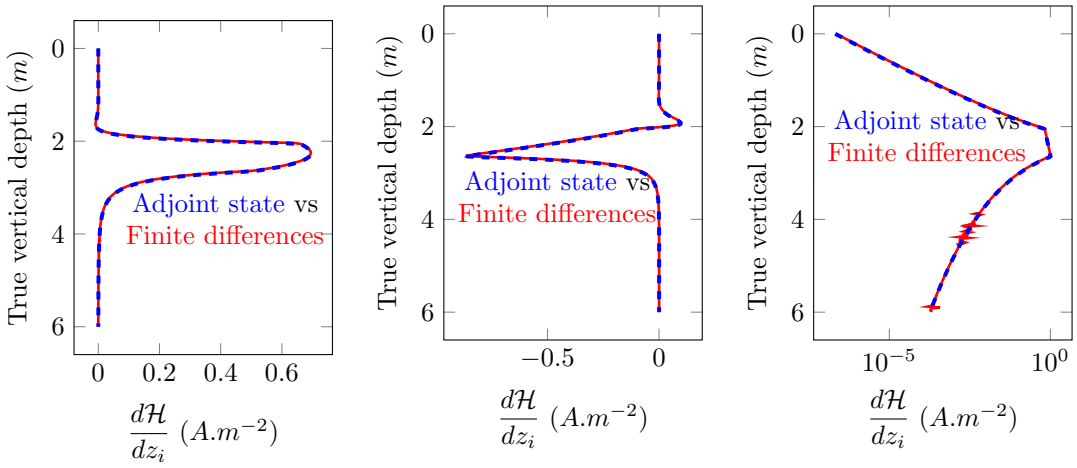

(A) Real part of the derivative (B) Imaginary part of the derivative (C) Absolute value of the derivative (log scale)

FIGURE 6. Model problem B. Derivative with respect to bed boundary position of the zz-component of the magnetic field for a vertical well.

6.2.2. *Model problem C: multi-layer media.* Figure 7 describes the logging instrument used for this model problem. In this example, the conductivity model features four layers. $\mathbf{z}_i = (z_{i,1}, z_{i,2}, z_{i,3})$ represents the location of the three interfaces. The conductivity of the media is $\boldsymbol{\sigma}_{\mathbf{z}_i} = \sigma_{\mathbf{z}_i}\mathbf{I}_3$, where:

$$\sigma_{\mathbf{z}_i}(\boldsymbol{x}) = \begin{cases} 1 & Sm^{-1} & \text{if } 0 < z < z_{i,1} \\ 10^{-2} & Sm^{-1} & \text{if } z_{i,1} \leq z < z_{i,2}, \\ 1 & Sm^{-1} & \text{if } z_{i,2} \leq z < z_{i,3} \\ 10^{-2} & Sm^{-1} & \text{if } z_{i,3} \leq z < 10, \end{cases} \tag{54}$$

with $\mathbf{z}_i = (3, 5, 7)$.

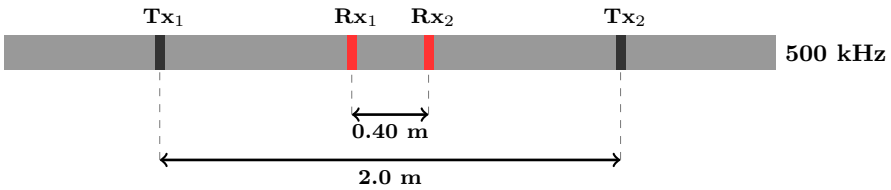

FIGURE 7. Model problem C. Logging instrument. Rx_1 and Rx_2 are the first and the second receivers, respectively. Tx_1 and Tx_2 are the first and the second transmitters, respectively.

For this problem, we consider the attenuation and the phase difference of the magnetic field between the two receivers. These are the quantities often recorded in borehole geophysical measurements. For details, see Appendix A.

Figure 8 describes the attenuation and the phase difference for the zz-component of the magnetic field. Figures 9 and 10 show the derivatives of the attenuation and the phase difference with respect to all bed boundary positions of the media using the adjoint state formulation vs those obtained with a finite difference method. As shown in the figures, the derivatives using the adjoint state method coincide with the finite differences ones for all cases. Indeed, the adjoint-based derivatives produce enhanced accuracy (see Figure 11 displaying a zoom of the derivative). Additionally, the adjoint-based method only requires the solution of one finite element problem with two right hand sides, while the finite differences approach involves the solution of one additional problem per interface (i.e., a total of $N_{int} + 1$ problems, where N_{int} is the number of interfaces whose derivative is estimated).

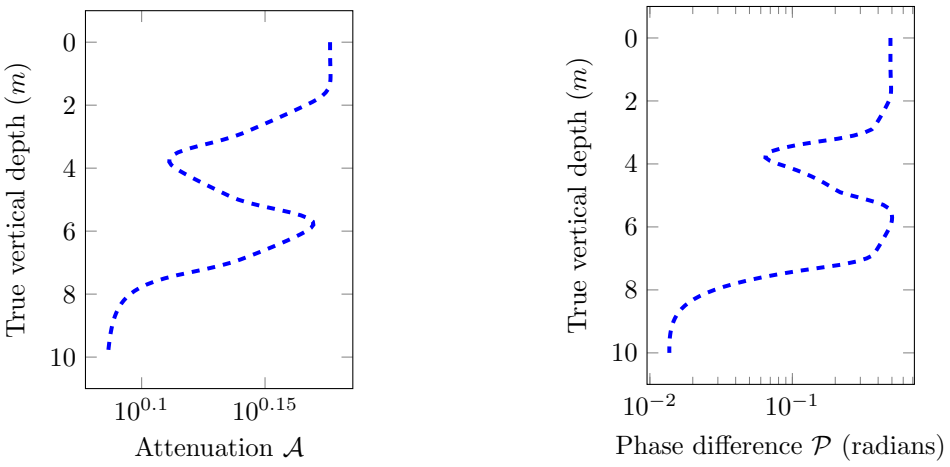

FIGURE 8. Model problem C. Attenuation and phase difference for the zz-component of the magnetic field.

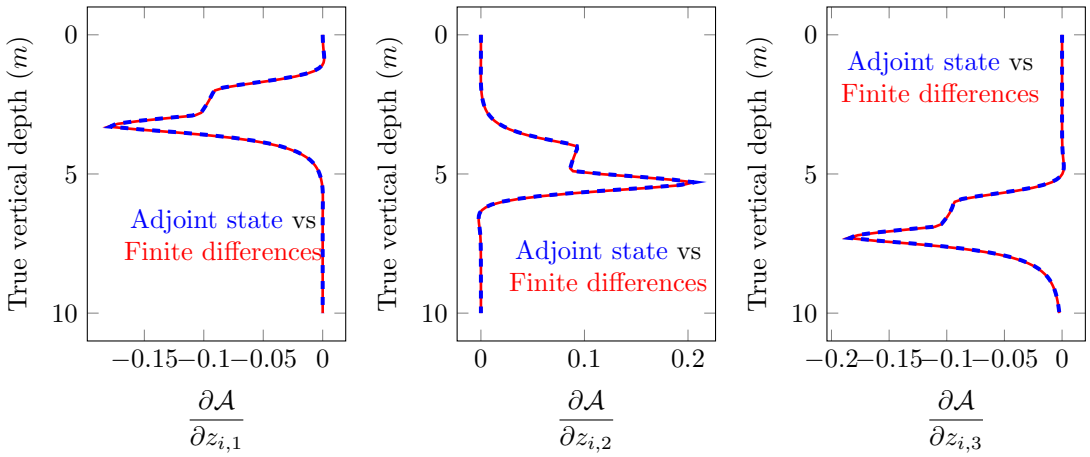

(A) First interface (B) Second interface (C) Third interface

FIGURE 9. Model problem C. Derivatives of the attenuation with respect to the bed boundary positions.

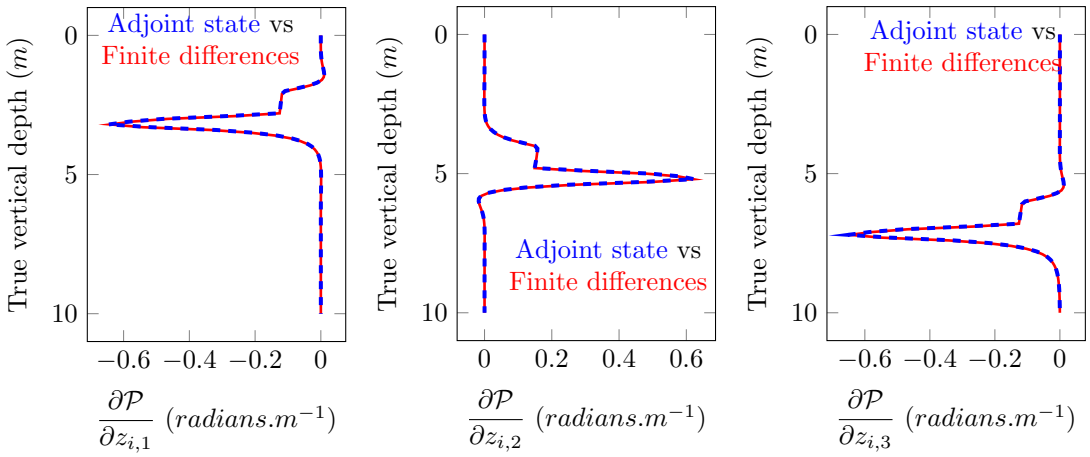

(A) First interface (B) Second interface (C) Third interface

FIGURE 10. Model problem C. Derivatives of the phase difference with respect to the bed boundary positions.

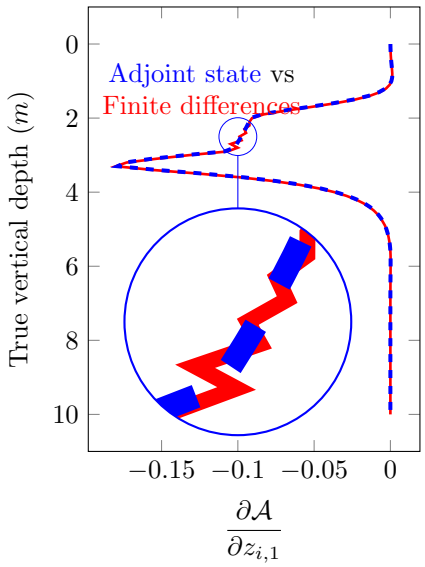

FIGURE 11. Model problem C. Derivative of the attenuation with respect to the first bed boundary position.

7. Conclusions

We have developed an adjoint-based formulation to compute the derivatives of geophysical resistivity measurements with respect to the bed boundary positions. The formulation is first deduced for the potential equation. Then, we extend the formulation to Maxwell's equations. We also consider a Hankel transform for the case of a 1D Earth model. We verified our formulations by comparing the numerical results with those obtained using an analytical solution for a potential equation and with a finite differences technique for a 1.5D Maxwell's system. Using the adjoint state method, we can compute the derivatives at (almost) no additional cost in time with respect to that needed to solve the forward problem, and we obtain an accurate evaluation of the derivatives.

8. Acknowledgement

This work has received funding from the European Union's Horizon 2020 research and innovation programme under the Marie Sklodowska-Curie grant agreement No 644602 and 777778, the Projects of the Spanish Ministry of Economy and Competitiveness with reference MTM2016-76329-R (AEI/FEDER, EU), and MTM2016-81697-ERC/AEI, the BCAM "Severo Ochoa" accreditation of excellence SEV-2013-0323, and the Basque Government through the BERC 2014-2017 program, and the Consolidated Research Group Grant IT649-13 on "Mathematical Modeling, Simulation, and Industrial Applications (M2SI)".

References

1. J. Alvarez-Aramberri and D. Pardo, *Dimensionally adaptive hp-finite element simulation and inversion of 2D magnetotelluric measurements*, Journal of Computational Science **18** (2017), 95–105.
2. S. A. Bakr and D. Pardo, *A multi-domain decomposition-based Fourier finite element method for the simulation of 3D marine CSEM measurements*, Computational Geosciences **21 (3)** (2017), 345–357.
3. S. A. Bakr, D. Pardo, and T. Mannseth, *Domain decomposition Fourier FE method for the simulation of 3D marine CSEM measurements*, J. Comput. Phys. **255** (2013), 456–470.
4. M. Bittar, J. Klein, R. Beste, G. Hu, M. Wu, , J. Pitcher, C. Golla, G. Althoff, M. Sitka, V. Minosyan, and M. Paulk, *A new azimuthal deep-reading resistivity tool for geosteering and advanced formation evaluation*, SPE Reservoir Evaluation and Engineering **12 (2)** (2009), 270–279.
5. S. Davydycheva and T. Wang, *A fast modelling method to solve Maxwell's equations in 1D layered biaxial anisotropic medium*, Geophysics **76 (5)** (2011), F293–F302.
6. L. Demkowicz, *Finite element methods for Maxwell equations. encyclopedia of computational mechanics*, John Wiley & Sons, Ltd, 2004.

7. O. Ijasan, C. Torres-Verdín, and W. E. Preeg, *Inversion-based petrophysical interpretation of logging-while-drilling nuclear and resistivity measurements*, Geophysics **78 (6)** (2013), D473–D489.
8. Y. Jia, G. L. Wang, and A. Abubakar, *Inversion for tilted triaxial conductivity in dipping layered formations*, IEEE (2015), 904 – 905, DOI:10.1109/APS.2015.7304839.
9. K. Key, *1D inversion of multicomponent, multifrequency marine CSEM data: Methodology and synthetic studies for resolving thin resistive layers*, Geophysics **74 (2)** (2009), F9–F20.
10. ———, *Is the fast hankel transform faster than quadrature?*, Computer Physics Communications **77 (3)** (2012), F21–F30.
11. J. A. Kong, *Electromagnetic wave theory*, Wiley-Interscience, 1986.
12. R. Lehe, M. Kirchen, I. A. Andriyash, B. B. Godfrey, and J. L. Vay, *quasi-cylindrical and dispersion-free Particle-in-cell algorithm*, Computer Physics Communications **203** (2013), 66–82.
13. L. O. Loseth and B. Ursin, *Electromagnetic fields in planarly layered anisotropic media*, Geophys. J. Int. **170** (2007), 44–F80.
14. A. Martí, *The role of electrical anisotropy in magnetotelluric responses: from modelling and dimensionality analysis to inversion and interpretation*, Surveys in Geophysics **35** (2014), 179–218.
15. D. Pardo and C. Torres-Verdin, *Fast 1D inversion of logging-while-drilling resistivity measurements for the improved estimation of formation resistivity in high-angle and horizontal wells*, Geophysics **80 (2)** (2014), E111–E124.
16. V. Puzyrev, J. Koldan, J. de la Puente, G. Houzeaux, M. Vzquez, and J. María-Cela, *A parallel finite-element method for three-dimensional controlled-source electromagnetic forward modelling*, Geophysical Journal International **193 (2)** (2013), 678–693.
17. M. Rabinovich, F. Le, J. Lofts, and S.Martakov, *The vagaries and myths of look around deep resistivity measurements while drilling*, Petrophysics **53 (2)** (2012), 86–101.
18. S. Rojas, I. Muga, and D. Pardo, *A quadrature-free method for simulation and inversion of 1.5D direct current (DC) borehole measurements*, Computational Geosciences **20 (6)** (2016), 1301–1318.
19. M. Shahriari, S. Rojas, D. Pardo, A. Rodríguez-Rozas, S. A. Bakr, V. M. Calo, and I. Muga, *A numerical 1.5D method for the rapid simulation of geophysical resistivity measurements*, submitted to Journal of Computational Physics, October 2017 (2017).
20. A. M. Tehrani and E. Slob, *Applicability of 1D and 2.5D marine controlled source electromagnetic modelling*, Geophysical Prospective **61** (2013), 602–613.
21. S. H. Ward and G. W. Hohmann, *Electromagnetic Methods in Applied Geophysics: volume 1, Theory*, Society of Exploration Geophysicists, 1987.

Appendix A. Derivatives of the attenuation and the phase difference

This Appendix depicts how to compute the derivatives of the attenuation and the phase difference with respect to the bed boundary positions. To simplify, we introduce the notation

$$\mathcal{H}_l^k = \mathcal{H}_{z_i,z}^k(Rx_l), \quad (1 \le k, l \le 2) \tag{55}$$

to denote the quantity measured at the receiver l when the transmitter k is active. For $l = 1, 2$, attenuation $\mathcal{A}^l$ and phase difference $\mathcal{P}^l$ are defined from $\mathcal{H}_1^l$ and $\mathcal{H}_2^l$ as:

$$\ln \frac{\mathcal{H}_1^l}{\mathcal{H}_2^l} = \underbrace{\ln \frac{\mid \mathcal{H}_1^l \mid}{\mid \mathcal{H}_2^l \mid}}_{\mathcal{A}^l} + i \underbrace{\left(ph(\mathcal{H}_1^l) - ph(\mathcal{H}_2^l)\right)}_{\mathcal{P}^l}, \tag{56}$$

where ph denotes the phase of a complex number. The final attenuation $\mathcal{A}$ and phase difference $\mathcal{P}$ are defined by averaging:

$$\mathcal{A} = \frac{1}{2}\left(\mathcal{A}^1 + \mathcal{A}^2\right), \quad \mathcal{P} = \frac{1}{2}\left(\mathcal{P}^1 + \mathcal{P}^2\right). \tag{57}$$

It remains to compute the derivative of $\mathcal{A}^l$ and $\mathcal{P}^l$ with respect to the position $z_{i,m}$ of the m^{th} bed boundary. We have

(58)

$$\mathcal{A}^l := \ln \frac{\mid \mathcal{H}_1^l \mid}{\mid \mathcal{H}_2^l \mid} = \ln \frac{\sqrt{\left(\mathcal{H}_1^{l,re}\right)^2 + \left(\mathcal{H}_2^{l,im}\right)^2}}{\sqrt{\left(\mathcal{H}_2^{l,re}\right)^2 + \left(\mathcal{H}_2^{l,im}\right)^2}} = \frac{1}{2}\ln\left[\left(\mathcal{H}_1^{l,re}\right)^2 + \left(\mathcal{H}_1^{l,im}\right)^2\right] - \frac{1}{2}\ln\left[\left(\mathcal{H}_2^{l,re}\right)^2 + \left(\mathcal{H}_2^{l,im}\right)^2\right]$$

where $\mathcal{H}_1 = \mathcal{H}_1^{l,re} + i\mathcal{H}_1^{l,im}$ and $\mathcal{H}_2 = \mathcal{H}_2^{l,re} + i\mathcal{H}_2^{l,im}$. Using the chain rule, we obtain:

$$\frac{\partial \mathcal{A}}{\partial z_{i,m}} = \frac{1}{\mid \mathcal{H}_1^l \mid^2}\left(\mathcal{H}_1^{l,re}\frac{\partial \mathcal{H}_1^{l,re}}{\partial z_{i,m}} + \mathcal{H}_1^{l,im}\frac{\partial \mathcal{H}_1^{l,im}}{\partial z_{i,m}}\right) - \frac{1}{\mid \mathcal{H}_2^l \mid^2}\left(\mathcal{H}_2^{l,re}\frac{\partial \mathcal{H}_2^{l,re}}{\partial z_{i,m}} + \mathcal{H}_2^{l,im}\frac{\partial \mathcal{H}_2^{l,im}}{\partial z_{i,m}}\right) \tag{59}$$

For the phase difference, it holds that

$$\mathcal{P}(\mathbf{z}_i) := ph(\mathcal{H}_1) - ph(\mathcal{H}_2) = \arctan\left(\frac{\mathcal{H}_1^{l,im}}{\mathcal{H}_1^{l,re}}\right) - \arctan\left(\frac{\mathcal{H}_2^{l,im}}{\mathcal{H}_2^{l,re}}\right). \tag{60}$$

Using again the chain rule, we obtain:

$$\frac{\partial \mathcal{P}}{\partial z_{i,m}} = \frac{1}{\mid \mathcal{H}_1^l \mid^2}\left(\mathcal{H}_1^{l,re}\frac{\partial \mathcal{H}_1^{l,im}}{\partial z_{i,m}} - \mathcal{H}_1^{l,im}\frac{\partial \mathcal{H}_1^{l,re}}{\partial z_{i,m}}\right) - \frac{1}{\mid \mathcal{H}_2^l \mid^2}\left(\mathcal{H}_2^{l,re}\frac{\partial \mathcal{H}_2^{l,im}}{\partial z_{i,m}} - \mathcal{H}_2^{l,im}\frac{\partial \mathcal{H}_2^{l,re}}{\partial z_{i,m}}\right). \tag{61}$$